Eigenwave based multiparameter traveltime expansions

ST 12.1

Martin Tygel (*), *Thilo Müiller* (**), *Peter Hubral* (**) *and Jörg Schleicher* (*)
(*) Depto. Matem. Aplicada, IMECC/UNICAMP, C.P. 6065, 13081-970, Campinas, SP, Brazil
(**) Geophys. Institut, Universität Karlsruhe, Hertzstr. 16, D-76187 Karlsruhe, Germany

Summary

Three different 2-D traveltime approximations for rays in the vicinity of a fixed zero-offset ray are presented and analyzed. All traveltimes are given as three-parameter expansions involving the emergence angle of the zero-offset ray with respect to the surface normal, as well as two wavefront curvatures associated with the zero-offset ray, namely the normal wave and normal-incidence-point wave. A comparison of all three multiparameter traveltime expansions is carried out and their potential for simulating zero-offset stack sections is discussed.

Introduction

Traveltimes of rays in the (paraxial) vicinity of a fixed (central) ray can be described by a certain number of parameters which refer only to the central ray only. The approximations are correct up to the second order of the distances between the paraxial and central rays at the corresponding initial and end points, independently of any seismic configuration. The traveltime approximations directly obtained from paraxial ray theory are the parabolic and the hyperbolic expansions (Schleicher et al., 1993). If the zero-offset ray is chosen as the central ray and assuming two-dimensional propagation, the parabolic and hyperbolic traveltimes can be expressed by simple three-parameter expressions, if the medium velocity at the coincident initial and end points (called central point) of the central ray is known. The three parameters are (a) the emergence angle β_0 of the zero-offset ray with respect to the surface normal, (b) the wavefront curvature K_N of the normal wave (N-wave), and (c) wavefront curvature K_{NIP} of the normal-incidence-point wave (NIP-wave). All these quantities being measured at the central point. As described in Hubral (1983), the normal and NIP waves are fictitious eigenwaves which have proven to be very useful for the description of zero-offset ray propagation. An appealing alternative traveltime expansion, also using the same three parameters β_0, K_N, and K_{NIP}, has been recently proposed by Gelchinsky et al. (1997). In this new representation, the paraxial rays can be specified so as to focus at a certain point of the zero-offset ray or at an extension to this ray. For this reason, Gelchinsky's expression has been referred to as the multi-focus traveltime. In the second-order approximation, also the multi-focus traveltime agrees with its parabolic and hyperbolic counterparts. In this paper, we provide simple derivations of all above-mentioned traveltime expressions and examine their behavior for some synthetic models. We also discuss the potential of these formulas for imaging procedures and inversion of the parameters involved, in particular for multi-focus, which has already been used for simulating zero-offset sections out of multi-coverage data.

Parabolic and hyperbolic traveltimes

In the following, we refer to Figure 1, which shows the (central)zero-offset ray that starts and ens at the central point X_0 and two paraxial rays from S, $\overline{S}$ to G, $\overline{G}$, respectively. They all cross at a fixed focus point P. The reflection point of the central ray is the normal incidence pointt (NIP).

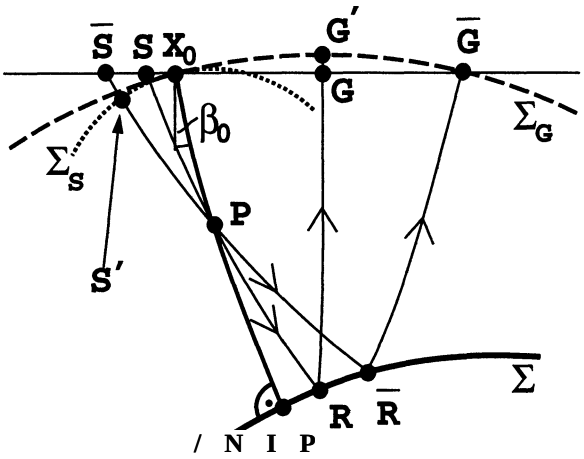

FIG. 1. Construction of the focusing wave. Shown is the normal ray from X_0 to NIP. Also depicted-are two of all possible paraxial rays (SRG and $\overline{\text{SRG}}$) that intersect this central ray at a common focus point P. These set of rays defines a fictitious wave called the focusing wave that starts at X_0 with the wavefront Σ_S, focuses at P, is reflected at the reflector Σ and emerges again at X_0, now with the wavefront Σ_G.

Following the formalism of Bortfeld (1989) tailored to the present two-dimensional propagation, the 2 x 2 *propgator matrix*

$$T = \begin{pmatrix} A & B \\ C & D \end{pmatrix}$$

describes a first-order relationship

$$\begin{cases} \Delta x_G = A\,\Delta x_S + B\,\Delta p_S\,, \\ \Delta p_G = C\,\Delta x_S + D\,\Delta p_S\,, \end{cases} \qquad (1)$$

where Δx_S and Δx_G are the source and receiver offsets of the paraxial ray with respect to the central ray. Δp_S and Δp_G denote the corresponding slowness projection differences of these rays onto the seismic line at the initial and end points, respectively. All these quantities are measured with respect to a fixed coordinate system attached to the tangent to the measurement surface at X_0. Using the fact that the downgoing segment of the

normal ray connnecting X_0 to NIP is the reverse ray to the upgoing segment from NIP to X_0 and along similar lines as in Hubral (1983) and Bortfeld (1989), we can find the useful relations

$$A = D = (K_{NIP} + K_N)/(K_{NIP} - K_N)\,, \tag{2}$$

$$B = (\cos^2 \beta_0/v)\,[2/(K_{NIP} - K_N)]\,. \tag{3}$$

The so-called *symplecticity* property of propagator matrices, namely the relation *AD* - *BC* = 1, produces the remaining element C. Following Bortfeld (1989) or Schleicher et al. (1993), we use midpoint and offset coordinates

$$x_m = \frac{\Delta x_G + \Delta x_S}{2}, \quad h = \frac{\Delta x_G - \Delta x_S}{2}, \tag{4}$$

to find for the parabolic traveltime

$$\begin{aligned} t_{par}(x_m, h) &= t_0 + (2\sin\beta_0/v)\,x_m \\ &+ (\cos^2\beta_0/v)\,(K_N\,x_m^2 + K_{NIP}\,h^2)\,, \end{aligned} \tag{5}$$

and for the hyperbolic traveltime

$$\begin{aligned} t_{hyp}^2(x_m, h) &= [t_0 + (2\sin\beta_0/v)\,x_m]^2 \\ &+ (2t_0\cos^2\beta_0/v)\,(K_N\,x_m^2 + K_{NIP}\,h^2)\,. \end{aligned} \tag{6}$$

In the above formulas, t_0 denotes the two way traveltime along the central ray.

Multi-focus traveltime

For the computation of the multi-focus traveltime we consider the bundle of primary reflection rays that focus a fixed point *P*. **As** depicted in Figure **1,** we imagine that all these rays describe a certain fictitious wave, which we call a *focusing wave.* For each of the focusing rays *SPRG,* the source and receiver offsets Δx_S and Δx_G are no longer independent but are related by the condition that the ray has to pass through the fixed point P. Our problem is to find a traveltime approximation for the rays paraxial to the central ray and satisfying this *focusing condition.* Let us now designate by Σ_S and Σ_G the initial and final wavefronts of the focusing wave, respectively. We approximate Σ_S by a circle, calling its curvature K_S and its curvature radius $r_S = 1/K_S$. Similarly, we define the curvature K_G and curvature radius $r_G = 1/K_G$ of the circular approximation of the wavefront Σ_G at the end point G. Let S' and G' denote the points where the focusing ray *SPRG* hits the initial and end wavefronts Σ_S and Σ_G, respectively. To investigate the situation in more detail, let us now consider the paraxial ray *SPRG* to be constituted by two ray segments. The first one connecting *S* to *P* and the second one describes the remaining path of the reflected ray from *P* to *R* and from there to G. We may then write the traveltimes t_S and t_G along these two ray segments ***SP*** and *PRG* in the form

$$t_S = t_{0S} + \Delta t_S\,, \quad t_G = t_{0G} + \Delta t_G\,, \tag{7}$$

where t_{0S} and Δt_S are the traveltimes along the ray segments $S'P$ and SS', respectively. The definitions of t_{0G} and Δt_G are analogous. Note that t_{0S} coincides with the traveltime along the central-ray segment from X_0 to *P* and t_{0G} coincides with the sum of the traveltimes along the central-ray segment from *P* to *NIP* and from ***NIP*** to X_0. Approximating the ray segments SS' and G'G by straight lines, we find, using simple geometrical arguments

$$\Delta t_S = \frac{r_S}{v}\left[\sqrt{1 + \frac{2\sin\beta_0}{r_S}\Delta x_S + \frac{\Delta x_S^2}{r_S^2}} - 1\right] \tag{8}$$

$$\Delta t_G = \frac{r_G}{v}\left[\sqrt{1 + \frac{2\sin\beta_0}{r_G}\Delta x_G + \frac{\Delta x_G^2}{r_G^2}} - 1\right]. \tag{9}$$

Our problem reduces, thus, to the determination of the curvature radii r_S and r_G, or equivalently their corresponding curvatures K_S or K_G. For that matter, we find it convenient to draw the line normal to the central ray at point *P* and consider it as an *auxiliary interface.* We also set a local coordinate system at *P* to locate ray points and slowness projections which refer to rays arriving to and leaving from this auxiliary interface. We may now define the two auxiliary propagator matrices

$$T_1 = \begin{pmatrix} A_1 & B_1 \\ C_1 & D_1 \end{pmatrix}\,, \quad T_2 = \begin{pmatrix} A_2 & B_2 \\ C_2 & D_2 \end{pmatrix}\,, \tag{10}$$

which correspond to the two (central) ray segments from X_0 to *P* and from *P* to X_0 being reflected at *NIP,* respectively. For the two segments *SP* and *PRG* of the paraxial ray *SPRG* (see Figure 1), the two matrices T_1 and T_2 set up the first-order relationships

$$\begin{cases} 0 = A_1\,\Delta x_S + B_1\,\Delta p_S\,, \\ \Delta p = C_1\,\Delta x_S + D_1\,\Delta p_S \end{cases} \tag{11}$$

and

$$\begin{cases} \Delta x_G = 0 + B_2\,\Delta p\,, \\ \Delta p_G = 0 + D_2\,\Delta p\,. \end{cases} \tag{12}$$

Note that the focusing condition at point *P* has been incorporated in the above equation systems by imposing the ray offsets of both segments *SP* and *SRG* at *P* to vanish and their slowness projections at *P* to be equal (denoted by Ap). Using simple algebra on the above equations provides a relationship between the source and receiver offsets for a focusing ray, namely

$$\Delta x_G = -\,(B_2/B_1)\,\Delta x_S\,. \tag{13}$$

The traveltimes t_1 and t_2, along the rays *SP* and *PRG* respectively, can be written, following Bortfeld (1989) and Hubral (1983),

$$t_1 = t_{0S} + \frac{\sin\beta_0}{v}\Delta x_S + \frac{\cos^2\beta_0\, K_S}{2v}(\Delta x_S)^2,$$
$$t_2 = t_{0G} + \frac{\sin\beta_0}{v}\Delta x_G + \frac{\cos^2\beta_0\, K_G}{2v}(\Delta x_G)^2, \qquad (14)$$

where t_{0S} and t_{0G} are the traveltimes along the respective central rays and

$$K_S = \frac{A_1}{B_1}\frac{v}{\cos^2\beta_0}, \quad K_G = \frac{D_2}{B_2}\frac{v}{\cos^2\beta_0}, \qquad (15)$$

are the wavefront curvatures of the fictitious focusing wave at the initial point S and end point G, respectively. To determine the quantities A_1/B_1 and D_2/B_2, we make use of the *chain rule* of propagator matrices $T = T_2\, T_1$, as well as the symplecticity relations $A_i\, D_i - B_i\, C_i = 1$, $(i = 1, 2)$. After some algebraic manipulation of the above equations, we find the relations $K_S = (A + B_2/B_1)/B$ and $K_G = (A + B_1/B_2)/B$. Together with the focusing condition, as well as the representations (2) and (3) of A and B in terms of K_N and K_{NIP}, we obtain the final result

$$K_S = r_S^{-1} = \frac{1}{1-\gamma}(K_N - \gamma\, K_{NIP}),$$
$$K_G = r_G^{-1} = \frac{1}{1+\gamma}(K_N + \gamma\, K_{NIP}), \qquad (16)$$

where

$$\gamma = (\Delta x_G - \Delta x_S)/(\Delta x_G + \Delta x_S) \qquad (17)$$

is the *focusing* parameter of Gelchinsky et al. (1997).

Numerical experiments

In order to illustrate the presented traveltime approximations, we have chosen a synthetic 2D-model, where a domelike structure is overlain by a smoothly curved interface as shown in Figure 2. Layer velocities are assumed to be constant, where v_1=2300m/s and v_2=2800m/s correspond to the first and second layer, respectively. The reflection response of the dome structure has been calculated by a ray tracing algorithm. The corresponding traveltime surface in dependence of midpoint and half-offset coordinates, x and h, respectively, is displayed in Figure 2 as well.

For a fixed midpoint coordinate x=–455m the traveltime approximations (given in formulas (5), (6) and (14)) are calculated for the reflected wavefield from the domelike reflector. Therefore the angle of incidence β_0 of the zero offset ray, as well as the radii of curvature $r_{NIP} = 1/K_{NIP}$ and $r_N = 1/K_N$ of the two eigenwaves need to be known. For the case of a known velocity model, simple geometrical considerations yield these parameters. In the present case these parameter are: $\beta_0 = 33.3°$, r_{NIP}=4852m and r_N=18407m. The resulting traveltime surfaces are given in Figure 3. In order to make comparison with the exact traveltimes visual, 2D-slices of the traveltime surfaces for constant half-offsets h=0m, 500m, 1000m, 2000m are depicted (see Figure 4).

For the zero-offset (h=0m) case it can be seen that all three traveltime approximations fit very good to the exact curve. Even away from the chosen midpoint (x=–455m) the results are good. For intermediate half-offset (h=500m, 1000m) the approximations are still very good for the hyperbolic and the multi-focus representation. The parabolic approximation is good at the chosen midpoint but deviates from the exact curve for distant midpoint coordinates. For larger offset (h=2000m) all three traveltime representations deviate from the exact traveltime response. However, the multi-focus traveltime approximation gives still a good fit on the branch for positive midpoints.

Discussion and Conclusions

Second- and higher-order traveltime expansions have been of great use for seismic processing for a long time. For CMP data, the one-parameter, hyperbolic NMO-traveltime is still routinely used for velocity analysis, stacking and inversion. More recently, and still for CMP data, two-parameter, fourth-order NMO-traveltime expansions are being used for more accurate results (see, e.g., Ross (1997) and also references therein).

Alternatively, using a full multi-coverage data set along a seismic line, three-parameter, second-order traveltime expansions can be used. In this paper, we have compared the parabolic and hyperbolic traveltimes derived from paraxial ray theory (see, e.g., Bortfeld, 1989; Schleicher et al., 1993) with the multi-focus traveltime of Gelchinsky et al. (1997). For this purpose, we have reformulated the three approximations in terms of the same three parameters, namely the emergence angle of the normal ray, as well as the wavefront curvatures of the N- and *NIP*-eigenwaves introduced by Hubral (1983). These seem to be the intrinsic parameters of the problem as they offer the potential of being further inverted for interval velocities (Hubral and Krey, 1980).

For various tested examples, the hyperbolic and multi-focus approximations gave, as expected consistently better results than the parabolic traveltime. It turned out that in most examples, including the one shown here, the multi-focus traveltime provided an even better approximation to the true reflection time than the hyperbolic one.

The fact that these three-paramter traveltime representations provide quite reasonable approximations, not only for the CMP traveltime curve but for the full multi-coverage traveltime surface, demonstrates their potential for use in an improved stacking procedure. For each central point, data information will be stacked along a full traveltime surface instead of the CMP hyperbola only. The resulting stacked zero-offset section as obtained for the optimal parameter combination (according to a maximum coherency criterion) is bound provide a significantly better signal-to-noise enhancement than conventional NMO/stack.

References

Bortfeld, R., 1989, Geometrical ray theory: Rays and traveltimes in seismic systems (second-order approximation of the traveltimes): Geophysics 54, 342-349.

Gelchinsky, B., Berkovitch, A., and Keydar, S., 1997, Multifocusing Homeomorphic Imaging: Part 1. Basic concepts and formulas: Presented at the Special Course on Homeomorphic Imaging given by B. Gelchinsky on February, 1997 in Seeheim, Germany.

Hubral, P., and Krey, T., 1980, Interval velocities from seismic reflection time measurements: Soc. Expl. Geophys. Monograph.

Hubral, P., 1983, Computing true-amplitude reflections in a laterally inhomogeneous earth: Geophysics 48, 1051-1062.

Ross, C.P., 1997: AVO and nonhyperbolic moveout: a practical example. First Break, 15, no. 2, p. 43-48.

Schleicher, J., Tygel, M. and Hubral, P., 1993, Parabolic and hyperbolic paraxial two-point traveltimes in 3D media: Geophysical Prospecting, 41, 495-513.

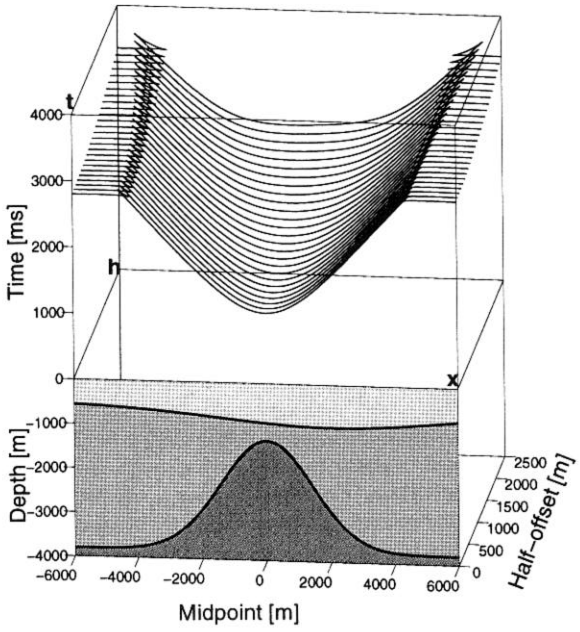

FIG. 2. The upper part shows the traveltime surface in the midpoint-half-offset domain as computed for the velocity structure depicted in the lower part.

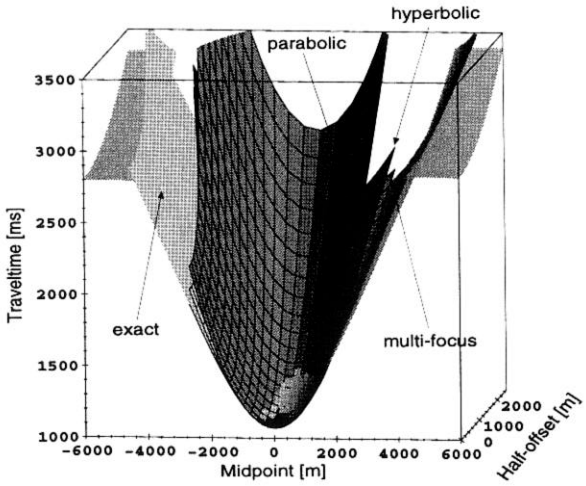

FIG. 3. The exact traveltime curve of Fig. 2 is compared to the three traveltime approximations discussed in the text, as computed for an arbitrarily chosen midpoint.

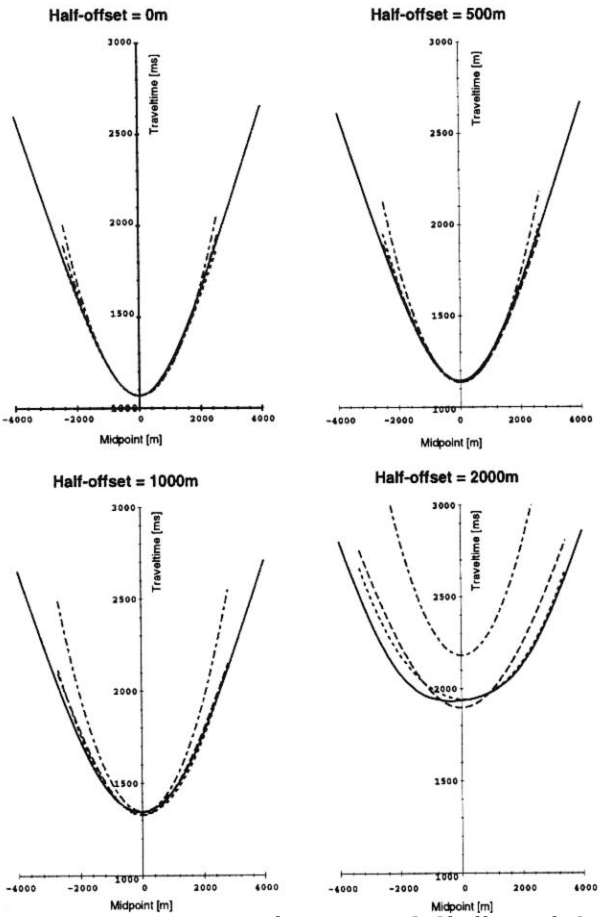

FIG, 4. 2D cross-cuts for constant half-offsets of the four traveltime surfaces of Fig. 3. For small offsets, all approximations are almost identical to the true traveltime (solid line). For greater offsets, the multi-focus traveltime (dotted line) approximates the true curve best. The hyperbolic approximation (dashed line) is a little worse, but much better than the parabolic one (dash-dotted line).